

A Dispersive Analysis of Low Energy $\gamma^*N \rightarrow \pi N$ Process

XIONG-HUI CAO¹, YAO MA¹, AND HAN-QING ZHENG^{1,2} *

¹*Department of Physics and State Key Laboratory of Nuclear Physics and Technology,
Peking University, Beijing 100871, P. R. China*

²*Collaborative Innovation Center of Quantum Matter, Beijing, Peoples Republic of China*

December 23, 2024

Abstract

We use a dispersion representation based on unitarity and analyticity to study the low energy $\gamma^*N \rightarrow \pi N$ process in the S_{11} channel. Final state interactions among the πN system are critical to this analysis. The left-hand part of the partial wave amplitude is imported from $\mathcal{O}(p^2)$ chiral perturbation theory result. On the right hand part, the final state interaction is calculated through Omnès formula in S -wave. It is found that good numerical fit can be achieved with only one subtraction parameter, and the electroproduction experimental data of multipole amplitudes E_{0+} , S_{0+} in the energy region below $\Delta(1232)$ are well described when the photon virtuality $Q^2 \leq 0.1\text{GeV}^2$. The γ^*N coupling of the possible sub-threshold resonance in S_{11} channel is also investigated.

1 Introduction

The electromagnetic interactions of nucleon have long been recognized as an important source of information for understanding strong interaction physics [1–7]. The investigation of pion photoproduction started in the 1950s with the seminal work of Chew, Goldberger, Low, and Nambu (CGLN) [1], where the formalism for pion photoproduction on nucleon target was developed, and fixed- t dispersion relations were used as a tool for the analyses of the reaction data. Postulates underlying the DR approach are analyticity, unitarity, and crossing symmetry of S -matrix. The CGLN formalism was later extended to pion electroproduction [8, 9], and DR was used in the analyses of the experimental data [9–12]. Based on the recent low energy experiments, partial wave analyses have been performed to study the underlying structure of the reaction amplitudes and describing the properties of the nucleon resonances [7, 13–15].

Since 1980s, it has been successful to explore the electroproduction and relevant processes using chiral perturbation theory (χ PT) at low energies [16–20]. For the calculation of loop diagrams, there are several renormalization schemes, which are e.g. heavy-baryon approach in Ref. [16] and EOMS scheme adopted in Refs. [17, 20], to solve the power-counting breaking (PCB) problems. However, χ PT only works well near the threshold and fails at slightly higher energies. So the unitary method is necessarily adopted in order to suppress the contributions from large energy and recast unitarity of the amplitude.

*Address after January 20: College of Physics, Sichuan University, Chengdu, Sichuan 610065, P. R. China

Some unitarity methods have already been explored (For a recent review, see Ref. [21]). The couple channel N/D method was used to unitarize χ PT amplitudes in Ref. [15], and Jülich model was adopted to study photoproduction and relevant process in Ref. [7]. In this paper, our $\gamma^*N \rightarrow \pi N$ amplitudes are obtained through the dispersive analysis [22], in the case we set up with chiral $\mathcal{O}(p^2)$ $\gamma^*N \rightarrow \pi N$ amplitudes and πN final state interaction estimated by the Omnès solution [23] in single channel approximation. In order to achieve such a dispersive analysis, efforts have been made in understanding the complicated analytic structure of the amplitudes.

Based on our dispersion representation, the multipole amplitudes ($S_{11}E_{0+}$ and $S_{11}S_{0+}$) data from Refs. [5, 13, 24–27] below the $\Delta(1232)$ peak have been fitted. This work extends our previous analyses on pion photoproduction [28], to the virtual-photon process with photon virtuality Q^2 up to 0.2GeV^2 , and find a good description of the data when $Q^2 \leq 0.1\text{GeV}^2$, with only one parameter. Besides, the comparison between the $\mathcal{O}(p^2)$ calculation in this paper and the one up to $\mathcal{O}(p^4)$ from Ref. [17] is performed and a discrepancy between the two results are noticed in higher Q^2 region.

In Refs. [29–31], evidences are found on the possible existence of a sub-threshold resonance named $N^*(890)$ in the S_{11} channel using the method proposed in Refs. [32–36], assisted by chiral amplitudes obtained in Refs. [37–40]. In this paper, further results are provided on γ^*N coupling to this resonance for future reference.

This paper is organized as follows. In section 2, a brief introduction to pion electroproduction is given. In section 3, we set up the dispersive formalism for $\gamma^*N \rightarrow \pi N$ process and make an analysis about the singularities which appear in this process. In section 4, numerical results of multipoles are carried out. In section 5, we calculate, in particular, the virtual-photon decay amplitudes at the pole, as introduced in Refs. [41, 42]. Finally we give our conclusions in section 6.

2 Pion electroproduction

2.1 Basics of single pion electroproduction off the nucleon

In this section we provide a short introduction to the notations describing the electroproduction of pions. Single pion electroproduction off the nucleon is the process described by

$$e(l_1) + N(p_1) \rightarrow e(l_2) + N(p_2) + \pi^a(q), \quad (1)$$

where a is the isospin index of the pion and $l_1(l_2)$, $p_1(p_2)$, q are incoming (outgoing) electron, incoming (outgoing) nucleon and pion momentum, respectively.

Due to the fact that the interaction between electron and nucleon is pure electromagnetic, for every additional virtual photon exchange, there will be one more fine structure constant $\alpha = e^2/(4\pi) \approx 1/137$ suppression factor. Hence we can only consider the lowest contribution or the so-called one-photon-exchange approximation, see Fig. 1.

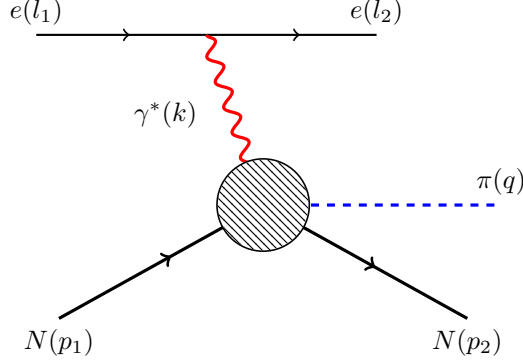


Figure 1: Pion electroproduction in the one-photon-exchange approximation. $k = l_1 - l_2$ represents the momentum of the single exchanged virtual photon. The shaded circle represents the full hadronic vertex.

In this approximation, the invariant amplitude \mathcal{M} is interpreted as the product of the polarization vector ϵ_μ of the virtual photon and the hadronic transition current matrix element \mathcal{M}^μ ,

$$\mathcal{M} = \epsilon_\mu \mathcal{M}^\mu = e \frac{\bar{u}(l_1) \gamma_\mu u(l_2)}{k^2} \mathcal{M}^\mu, \quad (2)$$

where

$$\mathcal{M}^\mu = -ie \langle N(p_2), \pi(q) | J^\mu(0) | N(p_1) \rangle, \quad (3)$$

with J^μ the electromagnetic current operator. Since $k^\mu \epsilon_\mu = 0$ in both photoproduction and electroproduction, it is possible to separate the pure electromagnetic part of the process from the hadronic part which is the process

$$\gamma^*(k) + N(p_1) \rightarrow N(p_2) + \pi(q), \quad (4)$$

where γ^* refers to a (space-like) virtual photon, so we can define $k^2 = -Q^2 < 0$, and Q^2 called photon virtuality. Mandelstam variables s , t and u are defined as

$$s = (p_1 + k)^2, \quad t = (p_1 - p_2)^2, \quad u = (p_1 - q)^2, \quad (5)$$

and satisfy $s + t + u = 2m_N^2 + m_\pi^2 - Q^2$, where m_N and m_π denote the nucleon mass and the pion mass, respectively. In the center-of-mass (cm) frame, πN final state system¹, the energies of the photon, k_0^* , the pion, E_π^* and incoming (outgoing) nucleon, E_1^* (E_2^*) are given by

$$\begin{aligned} k_0^* &= \frac{W^2 - Q^2 - m_N^2}{2W}, & E_\pi^* &= \frac{W^2 + m_\pi^2 - m_N^2}{2W}, \\ E_1^* &= \frac{W^2 + m_N^2 + Q^2}{2W}, & E_2^* &= \frac{W^2 + m_N^2 - m_\pi^2}{2W}, \end{aligned} \quad (6)$$

where $W = \sqrt{s}$ is the cm total energy. The values of the initial and final state momentum in the

¹In this section, the superscript $*$ refers to the physical quantity in the cm frame.

cm frame are

$$\begin{aligned} |\mathbf{k}^*| &= \sqrt{\left(\frac{W^2 - m_N^2 - Q^2}{2W}\right)^2 + Q^2}, \\ |\mathbf{q}^*| &= \sqrt{\left(\frac{W^2 - m_N^2 + m_\pi^2}{2W}\right)^2 - m_\pi^2}, \end{aligned} \quad (7)$$

The real photon equivalent energy in laboratory frame k^{lab} is given by

$$k^{\text{lab}} = \frac{W^2 - m_N^2}{2m_N}. \quad (8)$$

and $k^{\text{cm}} = (m_N/W)k^{\text{lab}}$. The cm scattering angle θ^* between the pion three-momentum and the z -axis, defined by the incoming photon direction, is depicted in Fig. 2

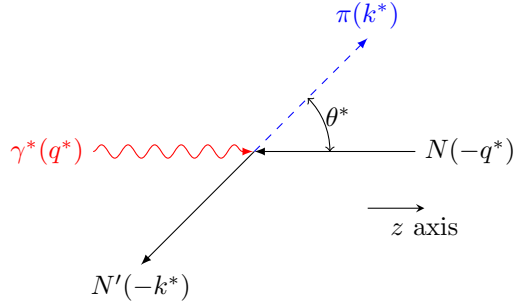


Figure 2: Scattering angle θ^* in the cm frame.

The scattering amplitude of pion electroproduction can be parametrized in terms of the Ball amplitudes [10], which are defined in Lorentz-covariant form

$$-ie \langle N' \pi | J^\mu(0) | N \rangle = \bar{u}(p_2) \left(\sum_{i=1}^8 B_i V_i^\mu \right) u(p_1), \quad (9)$$

where $u(p_1)$ and $\bar{u}(p_2)$ are the Dirac spinors of the nucleon in the initial and final states, respectively. Here we use the notation of [9, 16, 43], but slightly different from [2, 17]:

$$\begin{aligned} V_1^\mu &= \gamma_5 \gamma^\mu \not{k}, & V_2^\mu &= 2\gamma_5 P^\mu, & V_3^\mu &= 2\gamma_5 q^\mu, & V_4^\mu &= 2\gamma_5 k^\mu, \\ V_5^\mu &= \gamma_5 \gamma^\mu, & V_6^\mu &= \gamma_5 P^\mu \not{k}, & V_7^\mu &= \gamma_5 k^\mu \not{k}, & V_8^\mu &= \gamma_5 q^\mu \not{k}, \end{aligned} \quad (10)$$

where $P = (p_1 + p_2)/2$ and $\not{k} = \gamma^\mu k_\mu$. Using electromagnetic current conservation $k_\mu \mathcal{M}^\mu = 0$, only six independent amplitudes are required for the description of pion electroproduction. Furthermore, in pion photoproduction ($Q^2 = 0$) only four independent amplitudes survive.

The parameterization of Ref. [16] takes care of current conservation already from the beginning which contains only six independent amplitudes A_i ,

$$\mathcal{M}^\mu = \bar{u}(p_2) \left(\sum_{i=1}^6 A_i M_i^\mu \right) u(p_1) \quad (11)$$

with

$$\begin{aligned}
M_1^\mu &= \frac{1}{2}\gamma_5 (\gamma^\mu \not{k} - \not{k}\gamma^\mu) , \\
M_2^\mu &= 2\gamma_5 \left(P^\mu k \cdot \left(q - \frac{1}{2}k \right) - \left(q - \frac{1}{2}k \right)^\mu k \cdot P \right) , \\
M_3^\mu &= \gamma_5 (\gamma^\mu k \cdot q - \not{k}q^\mu) , \\
M_4^\mu &= 2\gamma_5 (\gamma^\mu k \cdot P - \not{k}P^\mu) - 2m_N M_1^\mu , \\
M_5^\mu &= \gamma_5 (k^\mu k \cdot q - k^2 q^\mu) , \\
M_6^\mu &= \gamma_5 (k^\mu \not{k} - k^2 \gamma^\mu) .
\end{aligned} \tag{12}$$

Each of them individually satisfies gauge invariance $k_\mu M_i^\mu = 0$. The scalar functions A_i and B_i can be linked through

$$\begin{aligned}
A_1 &= B_1 - m_N B_6 , \quad A_2 = \frac{2}{m_\pi^2 - t} B_2 , \quad A_3 = -B_8 , \quad A_4 = -\frac{1}{2} B_6 , \quad A_6 = B_7 , \\
A_5 &= \frac{2}{s + u - 2m_N^2} \left(B_1 - \frac{s - u}{2(m_\pi^2 - t)} B_2 + 2B_4 \right) = \frac{1}{k^2} \left(\frac{s - u}{t - m_\pi^2} B_2 - 2B_3 \right) .
\end{aligned} \tag{13}$$

The CGLN amplitudes \mathcal{F}_i are another common parameterization [1, 43], which plays an important role in experiments and partial wave analyses. These amplitudes are defined in the cm frame via

$$\epsilon_\mu \bar{u}(p_2) \left(\sum_{i=1}^6 A_i M_i^\mu \right) u(p_1) = \frac{4\pi W}{m_N} \chi_2^\dagger \mathbf{F} \chi_1 , \tag{14}$$

where χ_1 and χ_2 denote initial and final Pauli spinors, respectively. Electromagnetic current conservation allows us to work in the gauge where the polarization vector of virtual photon has a vanishing longitudinal component. In terms of the polarization vector of Eq. (2) this is achieved by introducing the vector [16, 44, 45]

$$b_\mu = \epsilon_\mu - \frac{\boldsymbol{\epsilon} \cdot \hat{\mathbf{k}}}{|\mathbf{k}|} k_\mu , \tag{15}$$

where $b_0 \neq 0$, but $\mathbf{b} \cdot \hat{\mathbf{k}} = 0$ ($\hat{\mathbf{k}} = \mathbf{k}/|\mathbf{k}|$). \mathcal{F} may be written as ($\boldsymbol{\sigma} = (\sigma_1, \sigma_2, \sigma_3)$)

$$\begin{aligned}
\mathbf{F} &= i\boldsymbol{\sigma} \cdot \mathbf{b} \mathcal{F}_1 + \boldsymbol{\sigma} \cdot \hat{\mathbf{q}} \boldsymbol{\sigma} \cdot (\hat{\mathbf{k}} \times \mathbf{b}) \mathcal{F}_2 + i\boldsymbol{\sigma} \cdot \hat{\mathbf{k}} \hat{\mathbf{q}} \cdot \mathbf{b} \mathcal{F}_3 + i\boldsymbol{\sigma} \cdot \hat{\mathbf{q}} \hat{\mathbf{q}} \cdot \mathbf{b} \mathcal{F}_4 \\
&\quad - i\boldsymbol{\sigma} \cdot \hat{\mathbf{q}} b_0 \mathcal{F}_7 - i\boldsymbol{\sigma} \cdot \hat{\mathbf{k}} b_0 \mathcal{F}_8 .
\end{aligned} \tag{16}$$

We can connect A_i and \mathcal{F}_i through algebraic calculations, and the results can be found in Appendix B.

The CGLN amplitudes can be expanded into multipole amplitudes [43]

$$\begin{aligned}
\mathcal{F}_1 &= \sum_{l=0}^{\infty} \{ [lM_{l+} + E_{l+}] P'_{l+1}(x) + [(l+1)M_{l-} + E_{l-}] P'_{l-1}(x) \} , \\
\mathcal{F}_2 &= \sum_{l=1}^{\infty} \{ (l+1)M_{l+} + lM_{l-} \} P'_l(x) , \\
\mathcal{F}_3 &= \sum_{l=1}^{\infty} \{ [E_{l+} - M_{l+}] P''_{l+1}(x) + [E_{l-} + M_{l-}] P''_{l-1}(x) \} , \\
\mathcal{F}_4 &= \sum_{l=2}^{\infty} \{ M_{l+} - E_{l+} - M_{l-} - E_{l-} \} P''_l(x) , \\
\mathcal{F}_7 &= \sum_{l=1}^{\infty} [lS_{l-} - (l+1)S_{l+}] P'_l(x) = \frac{|\mathbf{k}^*|}{k_0^*} \mathcal{F}_6 , \\
\mathcal{F}_8 &= \sum_{l=0}^{\infty} [(l+1)S_{l+}P'_{l+1}(x) - lS_{l-}P'_{l-1}(x)] = \frac{|\mathbf{k}^*|}{k_0^*} \mathcal{F}_5 ,
\end{aligned} \tag{17}$$

with $x = \cos \theta = \hat{\mathbf{q}} \cdot \hat{\mathbf{k}}$, $P_l(x)$ the Legendre polynomial of degree l , $P'_l = dP_l/dx$ and so on. Subscript l denotes the orbital angular momentum of the pion-nucleon system in the final state. The multipoles $E_{l\pm}$, $M_{l\pm}$, and $S_{l\pm}$ are functions of the cm total energy W and the photon virtuality Q^2 , and refer to transversal electric, magnetic transitions and scalar transitions², respectively. The subscript l_{\pm} denotes the total angular momentum $j = l \pm 1/2$ in the final state. By inverting the above equations, the angular dependence can be completely figured out [9]:

$$\begin{aligned}
E_{l+} &= \int_{-1}^1 \frac{dx}{2(l+1)} \left[P_l \mathcal{F}_1 - P_{l+1} \mathcal{F}_2 + \frac{l}{2l+1} (P_{l-1} - P_{l+1}) \mathcal{F}_3 + \frac{l+1}{2l+3} (P_l - P_{l+2}) \mathcal{F}_4 \right] , \\
E_{l-} &= \int_{-1}^1 \frac{dx}{2l} \left[P_l \mathcal{F}_1 - P_{l-1} \mathcal{F}_2 - \frac{l+1}{2l+1} (P_{l-1} - P_{l+1}) \mathcal{F}_3 + \frac{l}{2l-1} (P_l - P_{l-2}) \mathcal{F}_4 \right] , \\
M_{l+} &= \int_{-1}^1 \frac{dx}{2(l+1)} \left[P_l \mathcal{F}_1 - P_{l+1} \mathcal{F}_2 - \frac{1}{2l+1} (P_{l-1} - P_{l+1}) \mathcal{F}_3 \right] , \\
M_{l-} &= \int_{-1}^1 \frac{dx}{2l} \left[-P_l \mathcal{F}_1 + P_{l-1} \mathcal{F}_2 + \frac{1}{2l+1} (P_{l-1} - P_{l+1}) \mathcal{F}_3 \right] , \\
S_{l+} &= \int_{-1}^1 \frac{dx}{2(l+1)} [P_{l+1} \mathcal{F}_7 + P_l \mathcal{F}_8] , \\
S_{l-} &= \int_{-1}^1 \frac{dx}{2l} [P_{l-1} \mathcal{F}_7 + P_l \mathcal{F}_8] .
\end{aligned} \tag{18}$$

The isospin structure of the scattering amplitude can be written as

$$A(\gamma^* + N \rightarrow \pi^a + N') = \chi_2^\dagger \left\{ \delta^{a3} A^{(+)} + i\epsilon^{a3b} \tau^b A^{(-)} + \tau^a A^{(0)} \right\} \chi_1 , \tag{19}$$

where τ_a ($a = 1, 2, 3$) are Pauli matrices. We can define the isospin transition amplitudes by $A^{I, I_3}(A^{\frac{3}{2}, \pm \frac{1}{2}}, A^{\frac{1}{2}, \pm \frac{1}{2}})$, where $\{I, I_3\}$ denote isospin of the final πN system. In the notation $|I, I_3\rangle$

²Sometimes the longitudinal multipoles are used instead of the scalar multipoles, they satisfies a relationship $L_{l\pm} = (k_0/|\mathbf{k}|)S_{l\pm}$

the isospin part of the state vectors for the nucleon and the pion is written as

$$|p\rangle = \left| \frac{1}{2}, +\frac{1}{2} \right\rangle, \quad |n\rangle = \left| \frac{1}{2}, -\frac{1}{2} \right\rangle, \quad (20)$$

$$|\pi^+\rangle = -|1, +1\rangle, \quad |\pi^0\rangle = |1, 0\rangle, \quad |\pi^-\rangle = |1, -1\rangle. \quad (21)$$

So isospin transition amplitudes can be obtained from $A^{(\pm)}$ and $A^{(0)}$ via

$$A^{\frac{3}{2}, \frac{1}{2}} = A^{\frac{3}{2}, -\frac{1}{2}} = \sqrt{\frac{2}{3}} \left(A^{(+)} - A^{(-)} \right), \quad (22)$$

$$A^{\frac{1}{2}, \frac{1}{2}} = -\sqrt{\frac{1}{3}} \left(A^{(+)} + 2A^{(-)} + 3A^{(0)} \right), \quad (23)$$

$$A^{\frac{1}{2}, -\frac{1}{2}} = \sqrt{\frac{1}{3}} \left(A^{(+)} + 2A^{(-)} - 3A^{(0)} \right). \quad (24)$$

In the one-photon-exchange approximation, the differential cross section can be factorized as [3, 4]

$$\frac{d\sigma}{d\mathcal{E}_2 d\Omega_l d\Omega_\pi^*} = \frac{\alpha}{2\pi^2} \frac{\mathcal{E}_2}{\mathcal{E}_1} \frac{1}{Q^2} \frac{k^{\text{lab}}}{1 - \epsilon} \frac{d\sigma_v}{d\Omega_\pi^*} \equiv \Gamma \frac{d\sigma_v}{d\Omega_\pi^*}, \quad (25)$$

where Γ is the flux of the virtual photon, $\mathcal{E}_{1,2}$ denote the energy of the initial and final electrons in the laboratory frame, respectively. The parameter ϵ expresses the transverse polarization of the virtual photon in the laboratory frame and it's an invariant under collinear transformations. In terms of laboratory electron variables, it is given by [3]

$$\epsilon = \left(1 + 2 \frac{\mathbf{k}^2}{Q^2} \tan^2 \left(\frac{\theta_l}{2} \right) \right)^{-1}, \quad (26)$$

where θ_l is the scattering angle of the electron in the laboratory frame. The virtual photon differential cross section, $d\sigma_v/d\Omega_\pi^*$, for an unpolarized target without recoil polarization can be written in the form [4]:

$$\begin{aligned} \frac{d\sigma_v}{d\Omega_\pi^*} &= \frac{d\sigma_T}{d\Omega_\pi^*} + \epsilon \frac{d\sigma_L}{d\Omega_\pi^*} + \sqrt{2\epsilon(1+\epsilon)} \frac{d\sigma_{LT}}{d\Omega_\pi^*} \cos \phi_\pi^* + \epsilon \frac{d\sigma_{TT}}{d\Omega_\pi^*} \cos 2\phi_\pi^* \\ &+ h \sqrt{2\epsilon(1-\epsilon)} \frac{d\sigma_{LT'}}{d\Omega_\pi^*} \sin \phi_\pi^* + h \sqrt{1-\epsilon^2} \frac{d\sigma_{TT'}}{d\Omega_\pi^*}, \end{aligned} \quad (27)$$

in which ϕ_π^* is the azimuthal angle of pion and h is the helicity of the incoming electron. For further details about Eq. (27), especially concerning polarization observables, we refer to Ref. [4]. If we integrate the dependence of azimuthal angle, at the end we will get

$$\sigma_v = \sigma_T + \epsilon \sigma_L. \quad (28)$$

In the following chapter, we will introduce χ PT as an effective field theory which allow us to calculate pion production. The upper limit for the cm total energy W , restricted by the fact that we only consider pion and nucleon degrees of freedom, is below the $\Delta(1232)$ resonance peak. Furthermore, through the experience gained by studying EM form factors [46, 47], the estimate of the upper limit of momentum transfers is $Q^2 \simeq 0.1 \text{ GeV}^2$ in χ PT [17, 48].

3 Partial wave amplitudes

3.1 χ PT amplitudes and unitarity method

We recalculated the pion electroproduction process close to threshold using χ PT up to $\mathcal{O}(p^2)$ and confirm the results of [16]. The invariant scalar functions can be extracted from full amplitudes. The results are listed in the Appendix A. for higher order $\mathcal{O}(p^3)$ contributions and the influence of $\Delta(1232)$ resonance, readers can refer to Ref. [20].

In the following part, superscripts and subscripts I, J (isospin, total angular momentum) are ignored for brevity. Considering final-state theorem [49] and using the dispersion relation, the unitarized S wave amplitude can be written as [22, 28, 50–56]

$$\mathcal{M}(s) = \mathcal{M}_L(s) + \Omega(s) \left(-\frac{s}{\pi} \int_{(m_\pi+m_N)^2}^{\infty} \frac{(\text{Im } \Omega(s')^{-1}) \mathcal{M}_L(s')}{s'(s'-s)} ds' + \mathcal{P}(s) \right), \quad (29)$$

where $\mathcal{P}(s)$ is subtraction polynomial. The amplitude \mathcal{M}_L only contains left hand cut singularity. Thus, the pion electroproduction amplitude $\mathcal{M}(s)$ is determined up to a polynomial. $\Omega(s)$ is the so-called Omnès function [23]:

$$\Omega_J^I(s) = \tilde{\mathcal{P}}(s) \exp \left[\frac{s}{\pi} \int_{(m_\pi+m_N)^2}^{\infty} \frac{\delta_J^I(s')}{s'(s'-s)} ds' \right] \quad (30)$$

with $\tilde{\mathcal{P}}$ representing a polynomial, reflecting the zeros of $\Omega(s)$ in the complex plane and $\delta_J^I(s)$ being the elastic πN partial wave phase shift.

For our calculation, we use the χ PT result to estimate \mathcal{M}_L , so as long as function $\Omega(s)$ is known, we can get the amplitude with correct unitarity and analyticity property.

3.2 Singularity structure of partial wave amplitudes

Applicability of the Omnès method to the amplitudes of interest relies on the ability to separate the amplitude into a piece having only a left-hand cut and a piece having only a right hand one. This, a priori, is not the case if the left-hand cuts overlapped with the unitary cut.

So we review the analytic structures arising in our calculation and find that the singularities in this virtual process are rather complicated than real photoproduction. There will be some additional cuts in the complex s plane, compared with the photoproduction one. we follow Ref. [57] which relying on the Mandelstam double spectral representation to illustrate the analytic structure of the partial wave amplitudes. According to crossing symmetry, one amplitude can simultaneously describe the three channels of s, t, u :

$$\begin{aligned} s: & \quad \gamma^* + N \rightarrow \pi + N', \quad \sigma_1 = M^2, \quad \rho_1 = (m + M)^2; \\ t: & \quad \gamma^* + \pi \rightarrow \bar{N} + N', \quad \sigma_2 = m^2, \quad \rho_2 = 4m^2; \\ u: & \quad \gamma^* + \bar{N}' \rightarrow \pi + \bar{N}, \quad \sigma_3 = M^2, \quad \rho_3 = (m + M)^2. \end{aligned} \quad (31)$$

Here, for brevity, we define $m = m_\pi, M = m_N, \sigma_i$ represent the the mass squares of strongly interacting intermediate bound states, and the continuous spectra will begin at ρ_i which is the threshold of two particle intermediate states. Note here that the Mandelstam variable t defined in the s plane is related to $z_s = \cos \theta$ via

$$\begin{aligned} t = -Q^2 + m^2 - \frac{(s - Q^2 - M^2)(s + m^2 - M^2)}{2s} \\ + \left\{ \left[s^2 + 2(Q^2 - M^2)s + (Q^2 + M^2)^2 \right] (s - s_L)(s - s_R) \right\}^{\frac{1}{2}} \frac{z_s}{2s}. \end{aligned} \quad (32)$$

With regard to dynamical cut positions of the partial wave T matrix, we first take the t channel as an illustration. The full amplitude can be written as a dispersion integral:

$$T(s, t) = \int_{\sigma_2}^{\infty} \frac{\mathcal{F}(s, t')}{t' - t} dt' , \quad (33)$$

where \mathcal{F} is a spectral function. The partial wave amplitude is the projection of the full amplitude onto rotation function d^J ,

$$\begin{aligned} T^J(s) &= \int_{-1}^1 dz_s d^J(z_s) \int_{\sigma_2}^{\infty} dt' \frac{\mathcal{F}(s, t')}{t' - t(s, z_s)} \\ &= \int_{\sigma_2}^{\infty} dt' \mathcal{F}(s, t') \int_{-1}^1 dz_s \frac{d^J(z_s)}{\alpha(t', s) - \beta(s)z_s} , \end{aligned} \quad (34)$$

where integration $\int_{\sigma_2}^{\infty}$ denotes the sum of the value at pole $t' = \sigma_2$ and $\int_{\rho_2}^{\infty}$. It can be proved that the final singularity only comes from the form in logarithmic function

$$\ln(\alpha + \beta) - \ln(\alpha - \beta) . \quad (35)$$

We classify all cuts as follows:

- unitary cut: $s \in [s_R, \infty)$ on account of the s -channel continuous spectrum;
- t -channel cut: the arc, on the left of $s = s_c$, stems from t -channel continuous spectrum for $4m^2 \leq t \leq 4M^2$;
- u -channel cut: $s \in (-\infty, s_u]$ with $s_u = \frac{M^3 - m^2 M - m(M^2 + Q^2)}{m + M}$ due to the u -channel continuous spectrum for $u \geq (m + M)^2$;
- t -channel cut from pion pole: due to t channel single pion exchange, and the branch points locate at $0, C_t, C_t^\dagger$;
- u -channel cut from nucleon pole: due to t channel single nucleon exchange, and the branch points located at $0, C_u, C_u^\dagger$.

where the branch points in the complex plane are (the other three cases are symmetric about the real axis)

$$C_t = M^2 - \frac{Q^2}{2} + i\sqrt{4M^2Q^2 - m^2Q^2 - \frac{Q^4}{4} + \frac{M^2}{m^2}Q^4} , \quad (36)$$

$$C_u = M^2 - \frac{1}{2} \frac{m^2}{M^2} Q^2 + i\sqrt{4m^2Q^2 - \frac{m^2}{M^2}m^2Q^2 + \frac{m^2}{M^2}Q^4 - \frac{1}{4} \left(\frac{m^2}{M^2} \right)^2 Q^4} . \quad (37)$$

The singularities caused by the pole exchanges of t, u channels are complicated but definitely separated from the unitarity cut.

Aside from the above dynamical singularities, there exist additional kinematical singularities from relativistic kinematics and polarization spinor of fermions, especially in an inelastic scattering process. These inelastic ones will naturally introduce some square-root functions in the partial wave amplitudes (or multipole amplitudes) which will cause the kinematical singularities. They provide some of the most obvious characteristics in the case of relativistic theory. Here kinematical cuts are introduced when the arguments of the square-root functions from Eq. (32)

are negative. All the involved arguments together with their corresponding domains with their variable less than zero are listed in Table 1.

Table 1: Arguments causing singularities

Arguments	Domain
s	$(-\infty, 0)$
$s - s_R$	$(-\infty, s_R)$
$s - s_L$	$(-\infty, s_L)$
$s^2 + 2(Q^2 - M^2)s + (Q^2 + M^2)^2$	$(M^2 - Q^2 \pm 2iMQ, M^2 - Q^2 \pm i\infty)$

There are some arbitrariness when fixing the cut position [58, 59]. For example, compare $\sqrt{(s - s_L)(s - s_R)}$ and $\sqrt{s - s_L}\sqrt{s - s_R}$, they may correspond to different cut structure. The former will have an extra cut, which is perpendicular to the real axis and passes the midpoint of s_L and s_R . So we choose the latter one to make sure that left cuts are lying on the real axis. In addition, there is a pole like singularity at M^2 comes from the fact that Eq. (17) has the $1/(s - M^2)$ term (See Appendix B), which will appear in partial wave amplitudes. Finally, there may be a pole derived from the gauge invariant amplitudes. Relations (13) has introduced the $1/(t - m^2)$ pole singularity, If we consider the partial wave integral, e.g.,

$$\int dz \frac{z}{(t(z) - m^2)(u(z) - M^2)} \propto \int dz \frac{z}{(a + bz)(c - bz)} \propto \frac{1}{a + c} \propto \frac{1}{s - M^2 + Q^2}, \quad (38)$$

where $a = -m^2M^2 + M^4 - m^2Q^2 + M^2Q^2 + m^2s - 2M^2s + Q^2s + s^2$, $c = m^2M^2 - M^4 + m^2Q^2 - M^2Q^2 - m^2s + Q^2s + s^2$, $b = \sqrt{s - s_L}\sqrt{s - s_R}\sqrt{s^2 + 2(Q^2 - M^2)s + (Q^2 + M^2)^2}$. So the possible additional singularities in our partial wave analysis are displayed in Fig. 3.

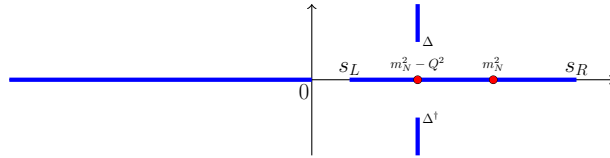


Figure 3: Kinematical singularities. The red dot represents the nucleon pole, and the two vertical solid rays represent the kinematic cuts from $\sqrt{s^2 + 2(Q^2 - M^2)s + (Q^2 + M^2)^2}$.

For a certain channel we are considering, these singularities may not all appear due to cancellation from linear combinations. Therefore, it must be analyzed in detail when it is used.

4 Numerical analyses

We are now in the position to compare the unitary representation of virtual photoproduction amplitude given in Eq. (29) with experimental multipole amplitude data in S_{11} channel. Here we use MAID2007 [13, 24] and DMT2001 [5, 25–27] results for fitting. These model provide a good description to multipole amplitudes, differential cross sections as well as polarization observables. They can be used as the basis for the prediction and the analysis of meson photo- and electroproduction data on proton and neutron targets.

4.1 Fitting procedure

In the fit, unknown parameters include the LECs appeared in $\mathcal{M}_{\chi PT}(s)$, the subtraction constants in the auxiliary function $\Omega(s)$ and the ones in the subtraction polynomial $\mathcal{P}(s)$. However, the parameters in chiral lagrangian appearing in $\mathcal{M}_{\chi PT}(s)$ up to $\mathcal{O}(p^2)$ are well fixed. They are $m_N = 0.9383$ GeV, $m_\pi = 0.1396$ GeV, $e = \sqrt{4\pi\alpha} = 0.303$, $g_A = 1.267$, $F_\pi = 0.0924$ GeV, $c_6 = 3.706/(4m_N)$ and $c_7 = -0.12/(2m_N)$ [60]³. Hence, $\mathcal{M}_{\chi PT}(s)$ is parameter free. Further, we set $\tilde{\mathcal{P}}(s) = 1$, and compute $\Omega(s)$ by using the partial wave phase shift extracted from the πN S matrix given in Ref. [61]. Note that it should be a good approximation for a single channel case that the integrations in Eqs. (30) and (29) are performed up to 2.1GeV^2 (below the ηN threshold). Lastly, the subtraction polynomial \mathcal{P} is taken to be a constant, $\mathcal{P}(s) = a$, i.e., here we only consider once subtraction.⁴ The above fit method is simultaneously performed on the data from the MAID and DMT models.

In the numerical analyses, we fit the multipole amplitudes with S_{11} channel from πN threshold to 1.440 GeV^2 just below the resonance $\Delta(1232)$. Since no error bars are given, we assign them according to Refs. [30,37]

$$\text{err}(\mathcal{M}_l^I) = \sqrt{\left(e_s^{R,I}\right)^2 + \left(e_r^{R,I}\right)^2} \left(\mathcal{M}_l^I\right)^2. \quad (39)$$

Here the superscripts R, I represent the real and imaginary parts of the amplitude. We choose $e_s^{R,I} = 0.4, 0.1[10^{-3}/m_\pi]$, $e_r^{R,I} = 10\%$. We take into account the errors caused by the model dependence of the partial wave data as much as possible [5,13]. The fit results to MAID2007 and DMT2001 data are displayed in Figs. 4, 5 and 6, 7, respectively. For comparison, we also show the $\mathcal{O}(p^2)$ chiral results of multipole amplitudes. As expected, the chiral results only describe the data at low energies close to threshold and in low Q^2 . The values of the fit parameters are collected in Table 2.

³Neglecting χ PT correction beyond tree level, the two LECs c_6 and c_7 can be related to the anomalous magnetic moments of the nucleon via $c_6 = (k_p + k_n)/2m_N$, $c_7 = (k_p - k_n)/4m_N$, with k_p and k_n being anomalous magnetic moments of proton and neutron, respectively. Since k_p and k_n are precisely determined by experiments, one can infer the uncertainties of c_6 and c_7 must be negligible and shall hardly change our results.

⁴The influence of twice subtractions $\mathcal{P}(s) = a + b s$ is also examined to test the fit result. It is found that the major physical outputs are almost inert.

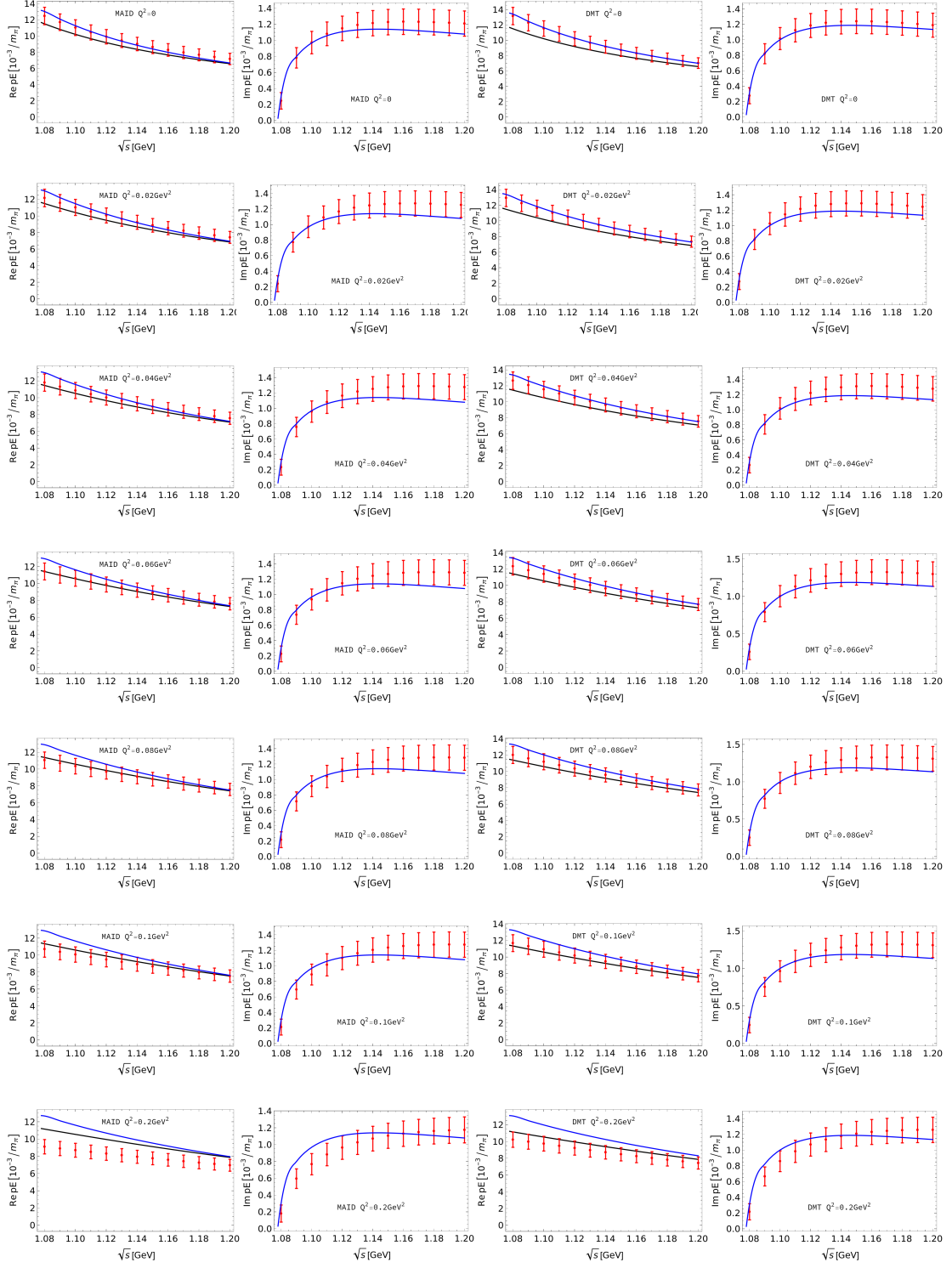


Figure 4: pE_{0+} : the two left columns correspond to the results of MAID, the others are from DMT. Moreover, the blue lines represent our fit result. For comparison, the chiral result is also shown (the black line).

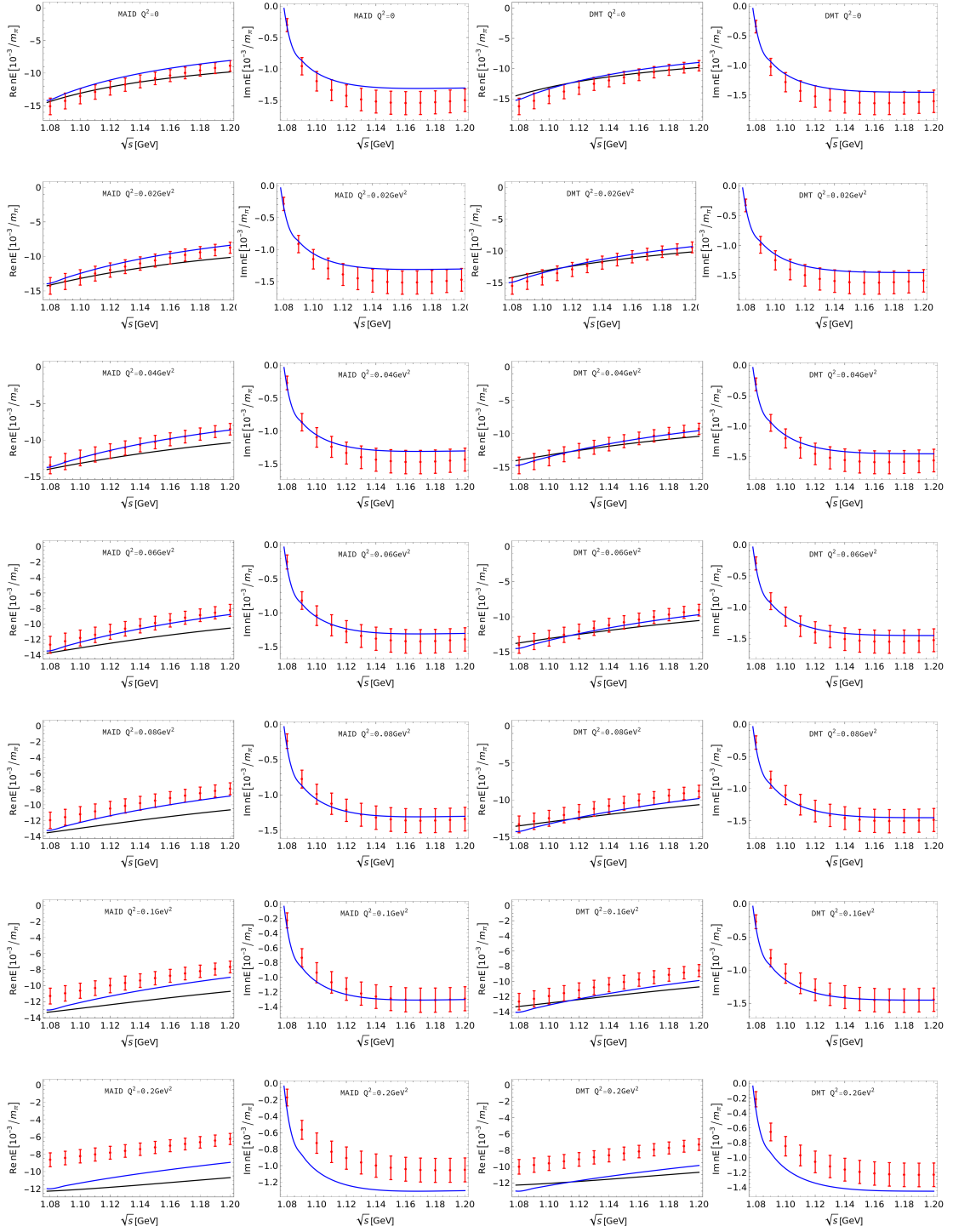


Figure 5: nE_{0+} : description the same as in Fig 4

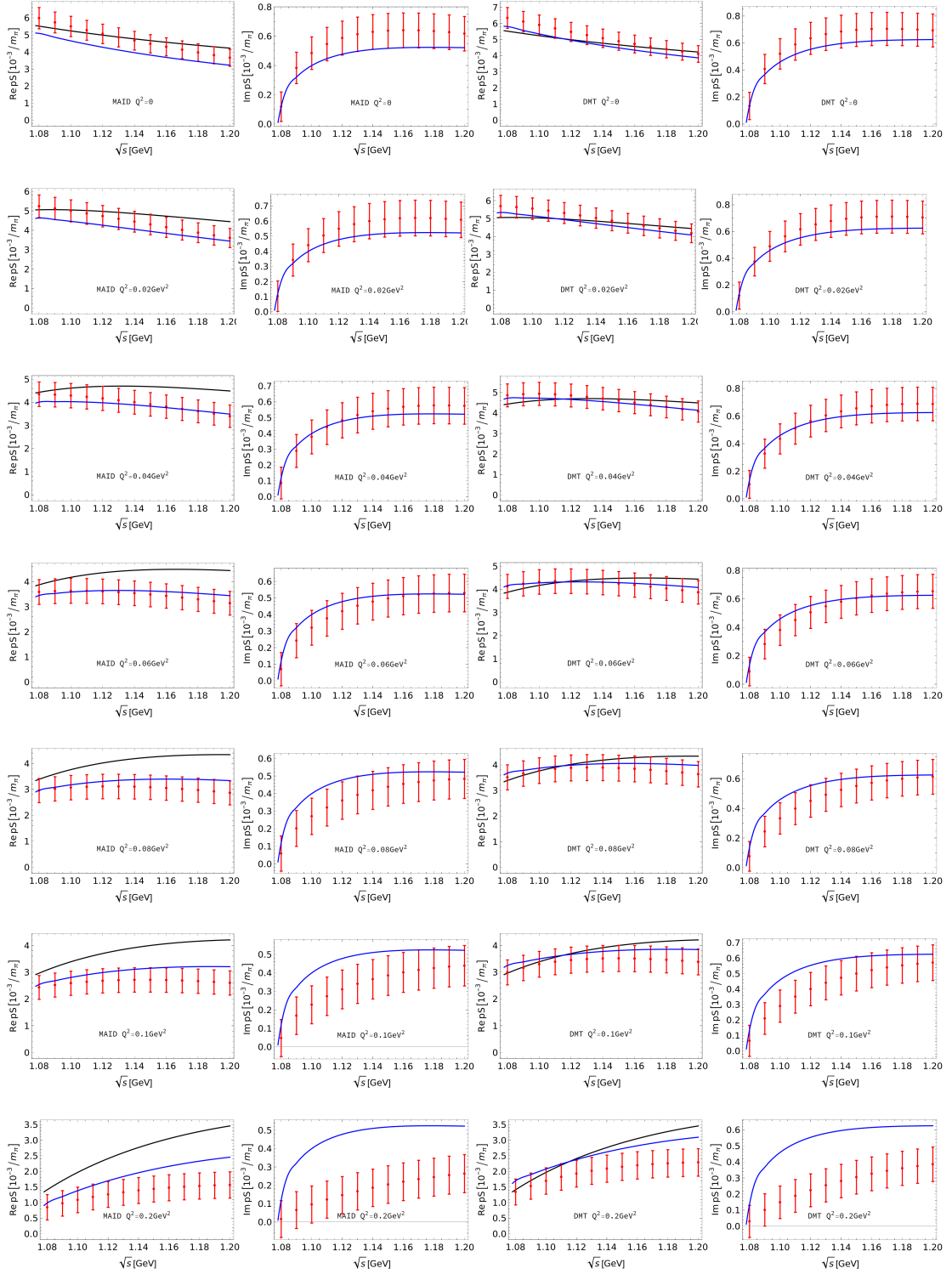


Figure 6: pS_{0+} : description the same as in Fig 4

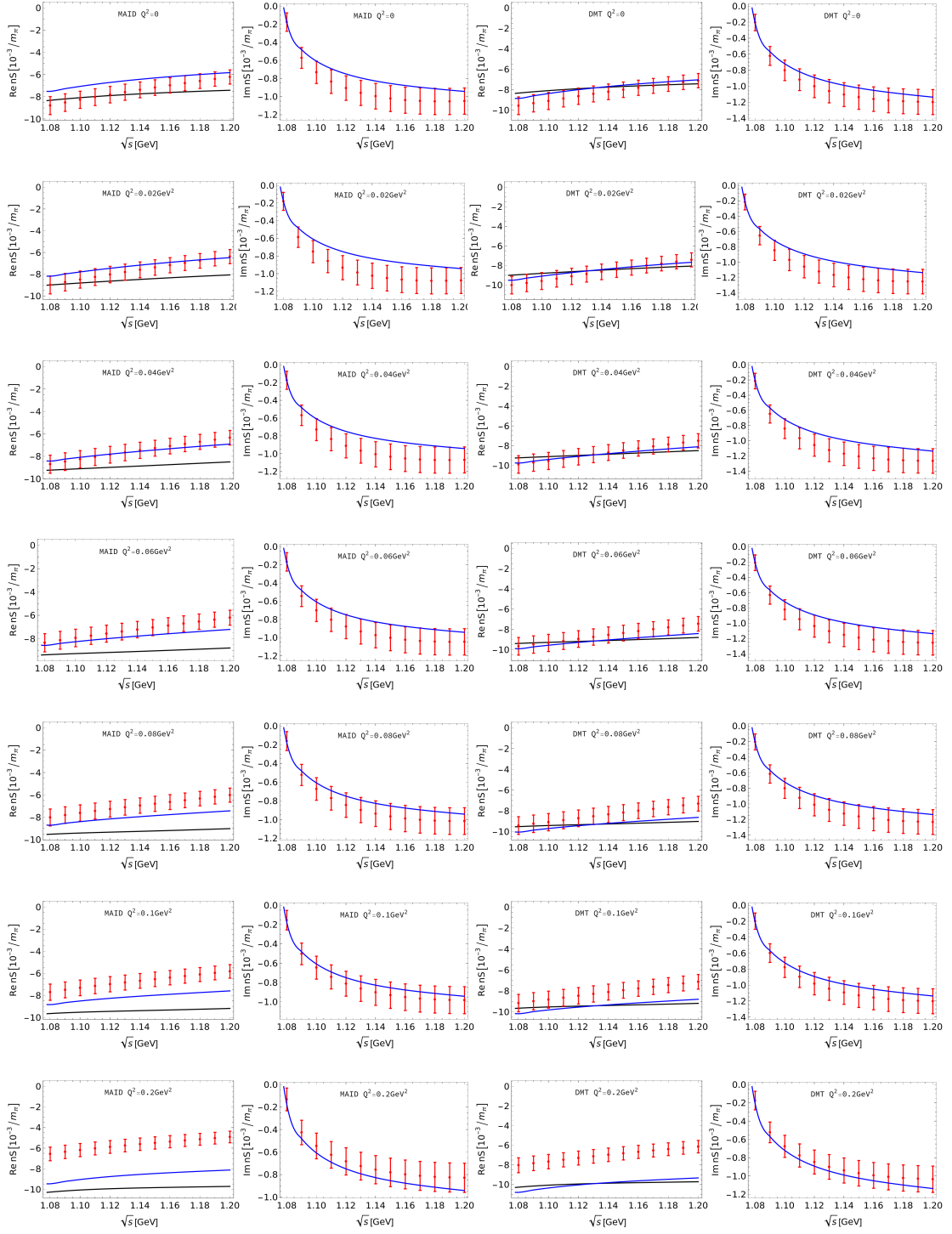


Figure 7: nS_{0+} : description the same as in Fig 4

Table 2: Fit results of once subtraction ($\mathcal{P} = a$). The parameter a is given in unit of $[10^{-3}/m_\pi]$.

Multipole	Target	Case	Value	$\chi^2/d.o.f$
E_{0+}	p	MAID	0.0635 ± 0.0546	0.59
		DMT	0.3857 ± 0.0411	0.32
	n	MAID	1.9389 ± 0.0664	0.74
		DMT	1.0762 ± 0.0593	0.51
S_{0+}	p	MAID	-1.0645 ± 0.0349	0.62
		DMT	-0.4647 ± 0.0281	0.36
	n	MAID	1.8815 ± 0.0680	1.27
		DMT	0.7558 ± 0.0606	0.82

In Figs. 4, 5 and 6, 7, we fit amplitudes from $Q^2 = 0$ to $Q^2 = 0.1\text{GeV}^2$ in the increments of 0.02GeV^2 . We also draw the result where $Q^2 = 0.2\text{GeV}^2$. It can be seen that, except that the fit to pS_{0+} is rather good, the other fit results do not improve much when $Q^2 = 0.2\text{GeV}^2$. This is within expectation that we did not consider corrections of vector meson exchanges. [46,47]. In general, as we can see in the Table 2, our results are in good agreement with the experimental data in the sense that the averaged χ^2 are close to one. Meanwhile, the central value of a is very small in any case. That can be understood by the fact that multipoles calculated from χPT and unitarity method can already well describe the experimental data. We also do the fit which uses a twice subtraction polynomial, i.e., $\mathcal{P} = a + bs$. However, the fit parameters a and b are found to be highly negative correlated. Thus, once subtraction is more advisable.

It is very convincing that no matter what data are used, the fit results of multipole amplitudes are very similar. The results can illustrate that our unitarity method is very powerful and effective in low energy regions and low Q^2 regions. But our results do not fit well in the case of high Q^2 . In our future work, we will consider using resonance χPT to improve the description ability of this method in high Q^2 .

4.2 remarks on results of Hilt et al.

Here we find that the $\mathcal{O}(p^4)$ results [17] and our amplitudes of multipole $S_{11}pE_{0+}$ different in higher Q^2 regions. Furthermore, $S_{11}nE_{0+}$, $S_{11}pS_{0+}$ and $S_{11}nS_{0+}$ are even different from our calculations at lower Q^2 . For comparison, we list UIM, DMT model, our results and that of [17].

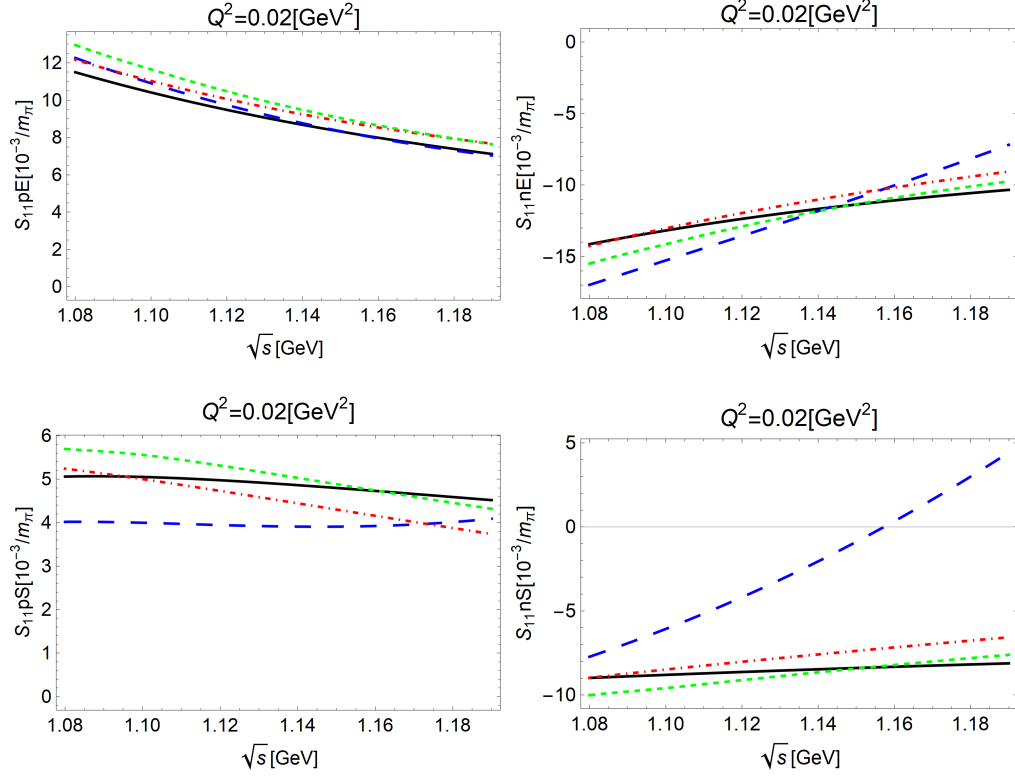


Figure 8: The black solid curves show our calculations at $\mathcal{O}(p^2)$ and the blue long-dashed curves are the outputs of the $\mathcal{O}(p^4)$ results [17]. The red dot-dashed and green short-dashed curves are the predictions of the UIM and the DMT model, respectively.

5 Electromagnetic couplings of the subthreshold resonance

5.1 Virtual-photon decay amplitudes at the pole

In the above subsection, all the involved parameters in the partial wave virtual photoproduction amplitude $\mathcal{M}_l(s)$ have been determined. Since $N^*(890)$, as a subthreshold resonance, is located on the second Riemann sheet (RS), one needs to perform analytic continuation in order to extract its couplings to the γ^*N and πN systems.

It can be proved that the residue can be extracted from [28]

$$g_{\gamma N} g_{\pi N} \simeq \frac{\mathcal{M}_l(s_p)}{\mathcal{S}'_l(s_p)}, \quad (40)$$

where $\mathcal{S}_l(s)$ corresponds to partial wave S matrix of elastic πN scattering. Residues $g_{\gamma N}$ and $g_{\pi N}$ denote the γN and πN couplings, respectively. The πN coupling can also be extracted from elastic πN scattering, i.e., $g_{\pi N}^2 \simeq \mathcal{T}_l(s_p)/\mathcal{S}'_l(s_p)$, where \mathcal{T}_l is the corresponding partial wave πN scattering amplitude. In order to compare the results with Refs. [41, 42], which are extracted

directly from multipole amplitudes parameterized in the \sqrt{s} plane, so we can write

$$E_{0+}^{\text{II}}(s \rightarrow s_p) \simeq \frac{g_{\gamma N}^E g_{\pi N}}{s - s_p} \simeq \frac{g_{\gamma N}^E g_{\pi N}}{2\sqrt{s_p}(\sqrt{s} - \sqrt{s_p})} = \frac{(g_{\gamma N}^E g_{\pi N}/2W_p)}{W - W_p}, \quad (41)$$

$$S_{0+}^{\text{II}}(s \rightarrow s_p) \simeq \frac{g_{\gamma N}^S g_{\pi N}}{s - s_p} \simeq \frac{g_{\gamma N}^S g_{\pi N}}{2\sqrt{s_p}(\sqrt{s} - \sqrt{s_p})} = \frac{(g_{\gamma N}^S g_{\pi N}/2W_p)}{W - W_p}, \quad (42)$$

where subscript p stands for pole parameters.

Using the above formulas, we can calculate the virtual-photon decay amplitudes $A_h^{\text{pole}}, S_{1/2}^{\text{pole}}$ at the $S_{11}N^*(890)$ pole position, which is Refs. [41, 42, 62]:

$$A_h^{\text{pole}} = C \sqrt{\frac{|\mathbf{q}_p|}{k_p^{\text{cm}}} \frac{2\pi(2J+1)W_p}{m_N \text{Res } \mathcal{T}_{\pi N}}} \text{Res } \mathcal{A}_\alpha^h, \quad (43)$$

$$S_{1/2}^{\text{pole}} = C \sqrt{\frac{|\mathbf{q}_p|}{k_p^{\text{cm}}} \frac{2\pi(2J+1)W_p}{m_N \text{Res } \mathcal{T}_{\pi N}}} \text{Res } \mathcal{S}_\alpha^{1/2}. \quad (44)$$

Refer to appendix C for the definition of $\mathcal{A}_\alpha^h, \mathcal{S}_\alpha^{1/2}$, here we use $\mathcal{A}_{0+}^{1/2} = -E_{0+}, \mathcal{S}_{0+}^{1/2} = -(1/\sqrt{2})S_{0+}$. Intuitively, $\mathcal{A}_\alpha^h, \mathcal{S}_\alpha^{1/2}$ characterize the power of electromagnetic couplings and the amplitudes of the “decay” process $N^* \rightarrow \gamma^* N$. $|\mathbf{q}_p|$ is the pion momenta at the pole. The factor C is $\sqrt{2/3}$ for isospin 3/2 and $-\sqrt{3}$ for isospin 1/2. So if we focus only on S_{11} channel, the corresponding virtual-photon decay amplitudes are given by

$$A_{1/2}^{\text{pole}}(Q^2) = g_{\gamma N}^E \sqrt{\frac{3\pi W_p}{m_N k_p^{\text{cm}}}}, \quad S_{1/2}^{\text{pole}}(Q^2) = g_{\gamma N}^S \sqrt{\frac{3\pi W_p}{2m_N k_p^{\text{cm}}}}. \quad (45)$$

It can be seen that the amplitudes, $\mathcal{A}_\alpha^{1/2}$ and $\mathcal{S}_\alpha^{1/2}$, as well as the residues, $A_{1/2}^{\text{pole}}$ and $S_{1/2}^{\text{pole}}$, are functions of the photon virtuality Q^2 .

5.2 Numerical results

According to Eqs. (40), $N^*(890)$ residues or couplings, $g_{\gamma N} g_{\pi N}$, can be extracted from multipole amplitudes E_{0+}, S_{0+} . In the meantime, $g_{\pi N}^2$ can be computed by using $g_{\pi N}^2 \simeq \mathcal{T}_l(s_p)/\mathcal{S}_l'(s_p)$, which was already obtained in Ref. [29]. We employed the MAID solution of the fit (The result of DMT is similar), and chose central value $\sqrt{s} = 0.882 - 0.190i$ for pole position to extract pole residues. $\mathcal{T}(s_p)$ can be obtained through $\mathcal{S}(s_p) = 1 + 2i\rho_{\pi N}(s_p)\mathcal{T}(s_p) = 0$ and $\frac{1}{\mathcal{S}'(s_p)}$ is just the residue of \mathcal{S}^{II} as explained Ref. [29].

The values of the decay amplitudes $A_{1/2}$ and $S_{1/2}$ at the pole position are shown in Figs. 9.

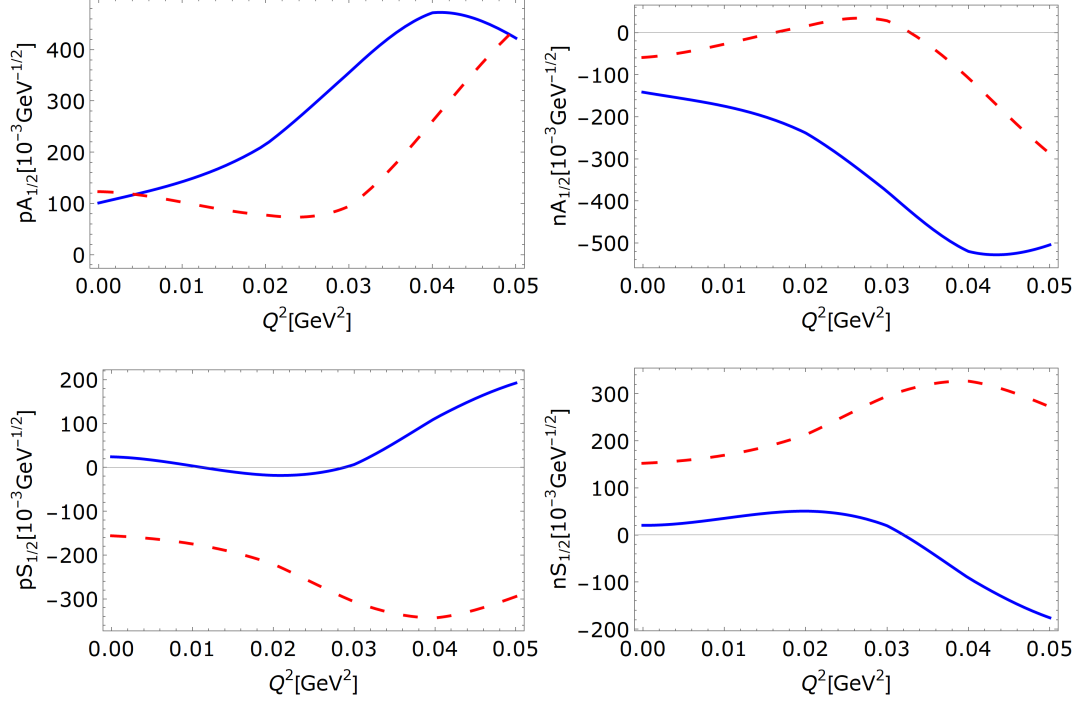


Figure 9: The blue solid line and the red solid line represent real and imaginary parts of virtual-photon decay amplitudes at pole position, respectively.

6 Summary

In this paper, we have performed a careful dispersive analysis about the process of single pion electroproduction off the nucleon in the S_{11} channel of the final πN system. In the dispersive representation, the right-hand cut contribution can be related to an Omnès solution, which takes the elastic πN phase shifts as inputs. At the same time, we estimate the left-hand cut contribution by making use of the $\mathcal{O}(p^2)$ amplitudes taken from χ PT. A detailed discussion on virtual photoproduction amplitude at the level of multipoles is presented. Different from Ref. [17, 20], here we go beyond pure χ PT calculations by applying the final state interaction theorem to partial wave amplitudes. To pin down the free parameters in the dispersive amplitude, we perform fits to experimental data of multipole amplitudes E_{0+} and S_{0+} for the energies ranging from πN threshold to 1.440 GeV². It is found that the experimental data can be well described by the dispersive amplitude with only one free subtraction parameter, when $Q^2 \leq 0.1 \text{ GeV}^2$. As Q^2 further increases to 0.2 GeV^2 , the fit fails, similar to what happened in other literature [17, 46, 47].

We also extend our analyses to study the property of $S_{11} N^*(890)$ as proposed recently in the literature. We analytically continue the dispersive amplitude to the second RS to extract the couplings of N^* to the $\gamma^* N$ and πN systems, and calculated the Q^2 dependence of them. Particularly, the decay amplitudes $A_{1/2}(Q^2)$ and $S_{1/2}(Q^2)$ at the $N^*(890)$ pole position are obtained. Our results serve providing further motivation for a new study of electromagnetic properties of $N^*(890)$.

Acknowledgments

The authors would like to thank De-Liang Yao, Yu-Fei Wang and Wen-Qi Niu for helpful discussions. This work is supported in part by National Nature Science Foundations of China (NSFC) under contract numbers 11975028 and 10925522.

Appendices

A Invariant amplitudes

$$\begin{aligned}
A_1^{(+)} &= -\frac{eg_A m_N}{2F} \left(\frac{1}{s - m_N^2} + \frac{1}{u - m_N^2} \right) - \frac{eg_A c_6}{F}, \\
A_2^{(+)} &= \frac{-eg_A m_N}{F} \frac{1}{t - m_\pi^2} \left(\frac{1}{s - m_N^2} + \frac{1}{u - m_N^2} \right), \\
A_3^{(+)} &= \frac{eg_A m_N c_6}{F} \left(\frac{1}{s - m_N^2} - \frac{1}{u - m_N^2} \right), \\
A_4^{(+)} &= \frac{eg_A m_N c_6}{F} \left(\frac{1}{s - m_N^2} + \frac{1}{u - m_N^2} \right), \\
A_5^{(+)} &= -\frac{eg_A m_N}{2F} \frac{1}{t - m_\pi^2} \left(\frac{1}{s - m_N^2} - \frac{1}{u - m_N^2} \right), \\
A_6^{(+)} &= 0, \\
A_1^{(-)} &= \frac{-eg_A m_N}{2F} \left(\frac{1}{s - m_N^2} - \frac{1}{u - m_N^2} \right), \\
A_2^{(-)} &= \frac{-eg_A m_N}{F} \frac{1}{t - m_\pi^2} \left(\frac{1}{s - m_N^2} - \frac{1}{u - m_N^2} \right), \\
A_3^{(-)} &= \frac{eg_A m_N c_6}{F} \left(\frac{1}{s - m_N^2} + \frac{1}{u - m_N^2} \right), \\
A_4^{(-)} &= \frac{eg_A m_N c_6}{F} \left(\frac{1}{s - m_N^2} - \frac{1}{u - m_N^2} \right), \\
A_5^{(-)} &= -\frac{eg_A m_N}{2F} \frac{1}{t - m_\pi^2} \left(\frac{1}{s - m_N^2} + \frac{1}{u - m_N^2} \right), \\
A_6^{(-)} &= 0, \\
A_1^{(0)} &= \frac{-eg_A m_N}{2F} \left(\frac{1}{s - m_N^2} + \frac{1}{u - m_N^2} \right) - \frac{eg_A c_7}{2F}, \\
A_2^{(0)} &= \frac{-eg_A m_N}{F} \frac{1}{t - m_\pi^2} \left(\frac{1}{s - m_N^2} + \frac{1}{u - m_N^2} \right), \\
A_3^{(0)} &= \frac{eg_A m_N c_7}{2F} \left(\frac{1}{s - m_N^2} - \frac{1}{u - m_N^2} \right), \\
A_4^{(0)} &= \frac{eg_A m_N c_7}{2F} \left(\frac{1}{s - m_N^2} + \frac{1}{u - m_N^2} \right), \\
A_5^{(0)} &= -\frac{eg_A m_N}{2F} \frac{1}{t - m_\pi^2} \left(\frac{1}{s - m_N^2} - \frac{1}{u - m_N^2} \right), \\
A_6^{(0)} &= 0,
\end{aligned} \tag{46}$$

where the two LECs F and g_A denote the chiral limit of pion decay constant and the axial-vector coupling constant, respectively. Here c_6 and c_7 are LECs of the $\mathcal{O}(p^2)$ chiral lagrangian.

B The relations between CGLN amplitudes and invariant amplitudes

The functions A_i and \mathcal{F}_i are connected with each other as the following relation [45, 63]:

$$\mathcal{F}_1 = (\sqrt{s} - m_N) \frac{N_1 N_2}{8\pi\sqrt{s}} \times \left[A_1 + \frac{k \cdot q}{\sqrt{s} - m_N} A_3 + \left(\sqrt{s} - m_N - \frac{k \cdot q}{\sqrt{s} - m_N} \right) A_4 - \frac{k^2}{\sqrt{s} - m_N} A_6 \right], \quad (47)$$

$$\mathcal{F}_2 = (\sqrt{s} + m_N) \frac{N_1 N_2}{8\pi\sqrt{s}} \frac{|\mathbf{q}||\mathbf{k}|}{(E_1 + m_N)(E_2 + m_N)} \times \left[-A_1 + \frac{k \cdot q}{\sqrt{s} + m_N} A_3 + \left(\sqrt{s} + m_N - \frac{k \cdot q}{\sqrt{s} + m_N} \right) A_4 - \frac{k^2}{\sqrt{s} + m_N} A_6 \right], \quad (48)$$

$$\mathcal{F}_3 = (\sqrt{s} + m_N) \frac{N_1 N_2}{8\pi\sqrt{s}} \frac{|\mathbf{q}||\mathbf{k}|}{E_1 + m_N} \left[\frac{m_N^2 - s + \frac{1}{2}k^2}{\sqrt{s} + m_N} A_2 + A_3 - A_4 - \frac{k^2}{\sqrt{s} + m_N} A_5 \right], \quad (49)$$

$$\mathcal{F}_4 = (\sqrt{s} - m_N) \frac{N_1 N_2}{8\pi\sqrt{s}} \frac{|\mathbf{q}|^2}{E_2 + m_N} \left[\frac{s - m_N^2 - \frac{1}{2}k^2}{\sqrt{s} - m_N} A_2 + A_3 - A_4 + \frac{k^2}{\sqrt{s} - m_N} A_5 \right], \quad (50)$$

$$\begin{aligned} \mathcal{F}_7 = & \frac{N_1 N_2}{8\pi\sqrt{s}} \frac{|\mathbf{q}|}{E_2 + m_N} \left[(m_N - E_1) A_1 - \left(\frac{|\mathbf{k}|^2}{2k_0} (2k_0\sqrt{s} - 3k \cdot q) - \frac{\mathbf{q} \cdot \mathbf{k}}{2k_0} (2s - 2m_N^2 - k^2) \right) A_2 \right. \\ & + (q_0(\sqrt{s} - m_N) - k \cdot q) A_3 + (k \cdot q - q_0(\sqrt{s} - m_N) + (E_1 - m_N)(\sqrt{s} + m_N)) A_4 \\ & \left. + (q_0 k^2 - k_0 k \cdot q) A_5 - (E_1 - m_N)(\sqrt{s} + m_N) A_6 \right], \end{aligned} \quad (51)$$

$$\begin{aligned} \mathcal{F}_8 = & \frac{N_1 N_2}{8\pi\sqrt{s}} \frac{|\mathbf{k}|}{E_2 + m_N} \left[(m_N + E_1) A_1 + \left(\frac{|\mathbf{k}|^2}{2k_0} (2k_0\sqrt{s} - 3k \cdot q) - \frac{\mathbf{q} \cdot \mathbf{k}}{2k_0} (2s - 2m_N^2 - k^2) \right) A_2 \right. \\ & + (q_0(\sqrt{s} + m_N) - k \cdot q) A_3 + (k \cdot q - q_0(\sqrt{s} + m_N) + (E_1 + m_N)(\sqrt{s} - m_N)) A_4 \\ & \left. + (q_0 k^2 - k_0 k \cdot q) A_5 - (E_1 + m_N)(\sqrt{s} - m_N) A_6 \right], \end{aligned} \quad (52)$$

with

$$N_i = \sqrt{E_i + m_N}, \quad E_i = \sqrt{\mathbf{p}_i^2 + m_N^2}, \quad i = 1, 2. \quad (53)$$

C Partial wave helicity amplitudes

In the following part, we introduce the partial wave helicity amplitude method of pion photo- and electroproduction [64].

It is convenient to perform partial wave projection using the helicity formalism proposed in Ref. [64, 65]. Here we define λ_i ($i = 1, 2, 3, 4$) which stand for the helicity of photon, initial nucleon, pion and final nucleon. For each set of helicity quantum numbers, denoted by $H_s \equiv \{\lambda_1 \lambda_2 \lambda_3 \lambda_4\}$, there is a helicity amplitude \mathcal{A}_{H_s} , which can be expanded as

$$A_{H_s}(s, t(\theta)) = 16\pi \sum_{J=M}^{\infty} (2J+1) A_{H_s}^J(s) d_{\lambda\mu}^J(\theta), \quad (54)$$

Table 3: Helicity amplitudes $\{A_{\mu\lambda}(\theta)\} = \{A_{H_s}\}$

$\mu \backslash \lambda$	$\lambda_1 = +1$		$\lambda_1 = -1$		$\lambda_1 = 0$	
	$\frac{3}{2}$	$\frac{1}{2}$	$-\frac{1}{2}$	$-\frac{3}{2}$	$\frac{1}{2}$	$-\frac{1}{2}$
$\frac{1}{2}$	H_1	H_2	H_4	$-H_3$	H_5	H_6
$-\frac{1}{2}$	H_3	H_4	$-H_2$	H_1	H_6	$-H_5$

where $M = \max\{|\lambda|, |\mu|\}$, $\lambda \equiv \lambda_1 - \lambda_2$ and $\mu \equiv \lambda_3 - \lambda_4 = -\lambda_4$, and $d^J(\theta)$ is the standard Wigner function. By imposing the orthogonal properties of the d functions, the partial wave helicity amplitudes $A_{H_s}^J(s)$ in the above equation may be projected, i.e.

$$A_{H_s}^J(s) = \frac{1}{32\pi} \int_{-1}^1 d\cos\theta A_{H_s}(s, t) d_{\lambda, \lambda'}^J(\theta) . \quad (55)$$

In particular, we use $H_i (i = 1 \sim 6)$ as symbols to define the helicity amplitude. The relations between $A_{\mu\lambda}$ and H_i are listed in Table. 3 [64].

The differential scattering cross section can be written as

$$\frac{d\sigma}{d\Omega} = \frac{1}{2} \frac{|\mathbf{q}|}{k^{\text{cm}}} \sum_{\lambda_i} |A_{\mu\lambda}|^2 . \quad (56)$$

From Eq. (56) and Table. 3, we can integrate the angle dependence

$$\sigma = 2\pi \frac{|\mathbf{q}|}{k^{\text{cm}}} \sum_J \sum_{i=1}^6 (2j+1) |H_i^J|^2 . \quad (57)$$

$A_{\mu\lambda}^J(H_i^J)$ has definite angular momentum but cannot be determined in parity. Therefore, we can add the final state with the opposite helicity $\mu, -\mu$ to obtain the so-called partial wave helicity parity eigenstates

$$\begin{aligned} A_{l+} &= -\frac{1}{\sqrt{2}} \left(A_{\frac{1}{2}, \frac{1}{2}(\lambda_1=1)}^J + A_{-\frac{1}{2}, \frac{1}{2}(\lambda_1=1)}^J \right) , \\ A_{(l+1)-} &= \frac{1}{\sqrt{2}} \left(A_{\frac{1}{2}, \frac{1}{2}(\lambda_1=1)}^J - A_{-\frac{1}{2}, \frac{1}{2}(\lambda_1=1)}^J \right) , \\ B_{l+} &= \sqrt{\frac{2}{l(l+2)}} \left(A_{\frac{1}{2}, \frac{3}{2}}^J + A_{-\frac{1}{2}, \frac{3}{2}}^J \right) \quad \ell \geq 1 , \\ B_{(l+1)-} &= -\sqrt{\frac{2}{l(l+2)}} \left(A_{\frac{1}{2}, \frac{3}{2}}^J - A_{-\frac{1}{2}, \frac{3}{2}}^J \right) \quad \ell \geq 1 , \\ S_{l+} &= -\frac{Q}{2|\mathbf{k}|} (l+1) \left(A_{\frac{1}{2}, \frac{1}{2}(\lambda_1=0)}^J + A_{-\frac{1}{2}, \frac{1}{2}(\lambda_1=0)}^J \right) , \\ S_{(l+1)-} &= -\frac{Q}{2|\mathbf{k}|} (l+1) \left(A_{\frac{1}{2}, \frac{1}{2}(\lambda_1=0)}^J - A_{-\frac{1}{2}, \frac{1}{2}(\lambda_1=0)}^J \right) . \end{aligned} \quad (58)$$

Notice that the normalization coefficients we use here are different from those in Refs. [66, 67], and $J = l + 1/2$ for ‘+’ amplitudes and $J = l - 1/2$ for ‘-’ amplitudes. A , B and S represent amplitudes with initial helicity of $1/2$, $3/2$, $1/2$, respectively, so it can also be written as $\mathcal{A}^{1/2}$, $\mathcal{A}^{3/2}$ and $\mathcal{S}^{1/2}$ up to some normalization factors, see Eq. (62).

Furthermore, with the definitions of Eqs. (54) and (55), then we can obtain

$$\begin{aligned}
H_1 &= \frac{1}{\sqrt{2}} \sin \theta \cos \frac{\theta}{2} \sum (B_{l+} - B_{(l+1)-}) (P_l'' - P_{l+1}'') , \\
H_2 &= \sqrt{2} \cos \frac{\theta}{2} \sum (A_{l+} - A_{(l+1)-}) (P_l' - P_{l+1}') , \\
H_3 &= \frac{1}{\sqrt{2}} \sin \theta \sin \frac{\theta}{2} \sum (B_{l+} + B_{(l+1)-}) (P_l'' + P_{l+1}'') , \\
H_4 &= \sqrt{2} \sin \frac{\theta}{2} \sum (A_{l+} + A_{(l+1)-}) (P_l' + P_{l+1}') , \\
H_5 &= \frac{Q}{|\mathbf{k}|} \cos \frac{\theta}{2} \sum (l+1) (S_{l+} + S_{(l+1)-}) (P_l' - P_{l+1}') , \\
H_6 &= \frac{Q}{|\mathbf{k}|} \sin \frac{\theta}{2} \sum (l+1) (S_{l+} - S_{(l+1)-}) (P_l' + P_{l+1}') .
\end{aligned} \tag{59}$$

According to the expansion method of CGLN [1], the relationship between helicity amplitudes and CGLN multipole amplitudes can also be obtained [1, 68]:

$$\begin{aligned}
H_1 &= -\frac{1}{\sqrt{2}} \sin \theta \cos \frac{\theta}{2} (\mathcal{F}_3 + \mathcal{F}_4) , \\
H_2 &= \sqrt{2} \cos \frac{\theta}{2} \left[(\mathcal{F}_2 - \mathcal{F}_1) + \frac{1}{2} (1 - \cos \theta) (\mathcal{F}_3 - \mathcal{F}_4) \right] , \\
H_3 &= \frac{1}{\sqrt{2}} \sin \theta \sin \frac{\theta}{2} (\mathcal{F}_3 - \mathcal{F}_4) , \\
H_4 &= \sqrt{2} \sin \frac{\theta}{2} \left[(\mathcal{F}_1 + \mathcal{F}_2) + \frac{1}{2} (1 + \cos \theta) (\mathcal{F}_3 + \mathcal{F}_4) \right] , \\
H_5 &= \cos \frac{\theta}{2} (\mathcal{F}_5 + \mathcal{F}_6) , \\
H_6 &= -\sin \frac{\theta}{2} (\mathcal{F}_5 - \mathcal{F}_6) .
\end{aligned} \tag{60}$$

Compare Eqs. (59) and (60) with the CGLN expansion, we have

$$\begin{aligned}
A_{l+} &= \frac{1}{2} [(l+2)E_{l+} + lM_{l+}] , \\
B_{l+} &= E_{l+} - M_{l+} , \\
A_{(l+1)-} &= -\frac{1}{2} [lE_{(l+1)-} - (l+2)M_{(l+1)-}] , \\
B_{(l+1)-} &= E_{(l+1)-} + M_{(l+1)-} .
\end{aligned} \tag{61}$$

$\mathcal{A}^h, \mathcal{S}^{1/2}$ can be related to the resonant part of the corresponding multipole amplitudes at the

pole position in the following way:

$$\begin{aligned}
\mathcal{A}_{l+}^{1/2} &= -\frac{1}{2} [(l+2)E_{l+} + lM_{l+}] , \\
\mathcal{A}_{l+}^{3/2} &= \frac{1}{2} \sqrt{l(l+2)} (E_{l+} - M_{l+}) , \\
\mathcal{S}_{l+}^{1/2} &= -\frac{l+1}{\sqrt{2}} S_{l+} , \\
\mathcal{A}_{(l+1)-}^{1/2} &= -\frac{1}{2} [lE_{(l+1)-} - (l+2)M_{(l+1)-}] , \\
\mathcal{A}_{(l+1)-}^{3/2} &= -\frac{1}{2} \sqrt{l(l+2)} (E_{(l+1)-} + M_{(l+1)-}) , \\
\mathcal{S}_{(l+1)-}^{1/2} &= -\frac{l+1}{\sqrt{2}} S_{(l+1)-} .
\end{aligned} \tag{62}$$

The scattering cross section is written in terms of \mathcal{A}_α^h as

$$\begin{aligned}
\sigma_T &= \left(\sigma_T^{1/2} + \sigma_T^{3/2} \right) + \epsilon \sigma_L , \\
\sigma_T^h &= 2\pi \frac{|\mathbf{q}|}{k^{\text{cm}}} \sum_{\alpha(\ell, J)} (2J+1) \left| \mathcal{A}_\alpha^h \right|^2 , \\
\sigma_L &= 2\pi \frac{|\mathbf{q}|}{k^{\text{cm}}} \frac{Q^2}{k^2} \sum_{\alpha(\ell, J)} (2J+1) \left| \mathcal{S}_\alpha^{1/2} \right|^2 ,
\end{aligned} \tag{63}$$

where superscript h stands for helicity. Expand the above formula, it can be obtained:

$$\begin{aligned}
\sigma_T^{1/2} &= 2\pi \frac{|\mathbf{q}|}{k^{\text{cm}}} \sum 2(l+1) \left[|A_{l+}|^2 + |A_{(l+1)-}|^2 \right] , \\
\sigma_T^{3/2} &= 2\pi \frac{|\mathbf{q}|}{k^{\text{cm}}} \sum \frac{l}{2} (l+1)(l+2) \left[|B_{l+}|^2 + |B_{(l+1)-}|^2 \right] , \\
\sigma_L &= 4\pi \frac{|\mathbf{q}|}{k^{\text{cm}}} \sum \frac{Q^2}{k^2} (l+1)^3 \left[|C_{l+}|^2 + |C_{(l+1)-}|^2 \right] .
\end{aligned} \tag{64}$$

References

- [1] G. F. Chew, M. L. Goldberger, F. E. Low, and Y. Nambu, Phys. Rev. **106**, 1345 (1957).
- [2] S. L. Adler, Annals Phys. **50**, 189 (1968).
- [3] E. Amaldi, S. Fubini, and G. Furlan, Springer Tracts Mod. Phys. **83**, 1 (1979).
- [4] D. Drechsel and L. Tiator, J. Phys. G **18**, 449 (1992).
- [5] V. Pascalutsa, M. Vanderhaeghen, and S. N. Yang, Phys. Rept. **437**, 125 (2007).
- [6] I. Aznauryan and V. Burkert, Prog. Part. Nucl. Phys. **67**, 1 (2012).
- [7] D. Rönnen *et al.*, Eur. Phys. J. A **50**, 101 (2014), [Erratum: Eur.Phys.J.A 51, 63 (2015)].
- [8] S. Fubini, Y. Nambu, and V. Wataghin, Phys. Rev. **111**, 329 (1958).
- [9] F. A. Berends, A. Donnachie, and D. L. Weaver, Nucl. Phys. **B4**, 1 (1967).
- [10] J. S. Ball, Phys. Rev. **124**, 2014 (1961).
- [11] R. Devenish and D. Lyth, Phys. Rev. D **5**, 47 (1972), [Erratum: Phys.Rev.D 6, 2067 (1972)].
- [12] R. Crawford and W. Morton, Nucl. Phys. B **211**, 1 (1983).
- [13] D. Drechsel, S. S. Kamalov, and L. Tiator, Eur. Phys. J. **A34**, 69 (2007).
- [14] M. Doring and K. Nakayama, Eur. Phys. J. A **43**, 83 (2010).
- [15] A. Gasparyan and M. Lutz, Nucl. Phys. **A848**, 126 (2010).
- [16] V. Bernard, N. Kaiser, T. S. H. Lee, and U.-G. Meissner, Phys. Rept. **246**, 315 (1994).
- [17] M. Hilt, B. C. Lehnhart, S. Scherer, and L. Tiator, Phys. Rev. **C88**, 055207 (2013).
- [18] D. L. Yao, L. Alvarez-Ruso, A. N. Hiller Blin, and M. J. Vicente Vacas, Phys. Rev. D **98**, 076004 (2018).
- [19] D. L. Yao, L. Alvarez-Ruso, and M. Vicente Vacas, Phys. Lett. B **794**, 109 (2019).
- [20] G. H. Guerrero Navarro and M. J. Vicente Vacas, Phys. Rev. D **102**, 113016 (2020).
- [21] D.-L. Yao, L.-Y. Dai, H.-Q. Zheng, and Z.-Y. Zhou, (2020), 2009.13495.
- [22] O. Babelon, J.-L. Basdevant, D. Caillerie, and G. Mennessier, Nucl. Phys. B **113**, 445 (1976).
- [23] R. Omnès, Nuovo Cim. **8**, 316 (1958).
- [24] D. Drechsel, O. Hanstein, S. Kamalov, and L. Tiator, Nucl. Phys. A **645**, 145 (1999).
- [25] S. Kamalov and S. N. Yang, Phys. Rev. Lett. **83**, 4494 (1999).
- [26] S. S. Kamalov, S. N. Yang, D. Drechsel, O. Hanstein, and L. Tiator, Phys. Rev. C **64**, 032201 (2001).
- [27] S. Kamalov, G.-Y. Chen, S.-N. Yang, D. Drechsel, and L. Tiator, Phys. Lett. B **522**, 27 (2001).

- [28] Y. Ma, W.-Q. Niu, D.-L. Yao, and H.-Q. Zheng, Chin. Phys. C **45**, 014104 (2021).
- [29] Y. F. Wang, D. L. Yao, and H. Q. Zheng, Chin. Phys. **C43**, 064110 (2019).
- [30] Y. F. Wang, D. L. Yao, and H. Q. Zheng, Front. Phys. **14**, 1 (2019).
- [31] Y. F. Wang, D. L. Yao, and H. Q. Zheng, Eur. Phys. J. **C78**, 543 (2018).
- [32] Z. G. Xiao and H. Q. Zheng, Nucl. Phys. **A695**, 273 (2001).
- [33] J. Y. He, Z. G. Xiao, and H. Q. Zheng, Phys. Lett. **B536**, 59 (2002), [Erratum: Phys. Lett. B549,362 (2002)].
- [34] H. Q. Zheng *et al.*, Nucl. Phys. **A733**, 235 (2004).
- [35] Z. Y. Zhou *et al.*, JHEP **02**, 043 (2005).
- [36] Z. Y. Zhou and H. Q. Zheng, Nucl. Phys. **A775**, 212 (2006).
- [37] Y. H. Chen, D. L. Yao, and H. Q. Zheng, Phys. Rev. **D87**, 054019 (2013).
- [38] J. Alarcon, J. Martin Camalich, and J. Oller, Annals Phys. **336**, 413 (2013).
- [39] D. L. Yao *et al.*, JHEP **05**, 038 (2016).
- [40] D. Siemens *et al.*, Phys. Rev. **C96**, 055205 (2017).
- [41] A. Švarc *et al.*, Phys. Rev. C **88**, 035206 (2013).
- [42] A. Švarc *et al.*, Phys. Rev. C **89**, 065208 (2014).
- [43] P. Dennery, Phys. Rev. **124**, 2000 (1961).
- [44] R. M. Davidson, Czech. J. Phys. **44**, 365 (1995).
- [45] B. Borasoy, P. C. Bruns, U.-G. Meissner, and R. Nissler, Eur. Phys. J. **A34**, 161 (2007).
- [46] B. Kubis and U. G. Meissner, Eur. Phys. J. C **18**, 747 (2001).
- [47] B. Kubis and U.-G. Meissner, Nucl. Phys. A **679**, 698 (2001).
- [48] L. Tiator *et al.*, Phys. Rev. C **94**, 065204 (2016).
- [49] K. M. Watson, Phys. Rev. **95**, 228 (1954).
- [50] Y. Mao, X. G. Wang, O. Zhang, H. Q. Zheng, and Z. Y. Zhou, Phys. Rev. **D79**, 116008 (2009).
- [51] R. Garcia-Martin and B. Moussallam, Eur. Phys. J. C **70**, 155 (2010).
- [52] B. Moussallam, Eur. Phys. J. C **73**, 2539 (2013).
- [53] I. V. Danilkin, M. F. M. Lutz, S. Leupold, and C. Terschlusen, Eur. Phys. J. C **73**, 2358 (2013).
- [54] I. Danilkin and M. Vanderhaeghen, Phys. Lett. B **789**, 366 (2019).
- [55] I. Danilkin, O. Deineka, and M. Vanderhaeghen, Phys. Rev. D **101**, 054008 (2020).

- [56] M. Hoferichter and P. Stoffer, JHEP **07**, 073 (2019).
- [57] J. Kennedy and T. Spearman, Phys. Rev. **126**, 1596 (1962).
- [58] M. Doring, C. Hanhart, F. Huang, S. Krewald, and U.-G. Meissner, Nucl. Phys. A **829**, 170 (2009).
- [59] S. Ceci *et al.*, Phys. Rev. C **84**, 015205 (2011).
- [60] M. Tanabashi *et al.*, Particle Data Group, Phys. Rev. **D98**, 030001 (2018).
- [61] M. Hoferichter, J. Ruiz de Elvira, B. Kubis, and U.-G. Meißner, Phys. Rept. **625**, 1 (2016).
- [62] N. Suzuki, T. Sato, and T.-S. Lee, Phys. Rev. C **82**, 045206 (2010).
- [63] B. Pasquini, D. Drechsel, and L. Tiator, Eur. Phys. J. **A34**, 387 (2007).
- [64] R. Walker, Phys. Rev. **182**, 1729 (1969).
- [65] M. Jacob and G. C. Wick, Annals Phys. **7**, 404 (1959), [Annals Phys.281,774(2000)].
- [66] F. A. Berends and A. Donnachie, Nucl. Phys. B **136**, 317 (1978).
- [67] R. Arndt, R. Workman, Z. Li, and L. Roper, Phys. Rev. C **42**, 1864 (1990).
- [68] L. Tiator, R. Workman, Y. Wunderlich, and H. Haberzettl, Phys. Rev. C **96**, 025210 (2017).